Micron 124 (2019) 102686

Contents lists available at ScienceDirect

Micron

journal homepage: www.elsevier.com/locate/micron

Mechanical characterisation of pentagonal gold nanowires in three different test configurations: A comparative study

Mikk Antsov[a], Boris Polyakov[b], Vahur Zadin[c], Magnus Mets[a], Sven Oras[a], Mikk Vahtrus[a], Rünno Lõhmus[a], Leonid Dorogin[a], Sergei Vlassov[a,*]

[a] Institute of Physics, University of Tartu, W. Ostwaldi Str. 1, 50412, Tartu, Estonia
[b] Institute of Solid State Physics, University of Latvia, Kengaraga 8, LV-1063, Riga, Latvia
[c] Institute of Technology, University of Tartu, Nooruse 1, 50411 Tartu, Estonia

ARTICLE INFO

Keywords:
Gold
Nanowires
Mechanical properties
Bending test
Finite element method

ABSTRACT

Mechanical characterisation of individual nanostructures is a challenging task and can greatly benefit from the utilisation of several alternative approaches to increase the reliability of results. In the present work, we have measured and compared the elastic modulus of five-fold twinned gold nanowires (NWs) with atomic force microscopy (AFM) indentation in three different test configurations: three-point bending with fixed ends, three-point bending with free ends and cantilevered-beam bending. The free-ends condition was realized by introducing a novel approach where the NW is placed diagonally inside an inverted pyramid chemically etched in a silicon wafer. In addition, all three configurations were simulated with a finite element method to obtain better insight into stress distribution inside NWs during bending depending on test conditions. The free-ends configuration yielded elastic modulus similar to a classical fixed-ends approach (88 ± 20 GPa vs 87 ± 16 GPa), indicating the reliability of the proposed method. At the same time, the free-ends configuration benefits from a more favourable NW position relative to the probe with facet facing upwards in contrast to the sharp edge in the case of fixed ends. From the other hand, the free-ends configuration was less suitable for strength measurements, as NW can run into the bottom of the inverted pyramid because of a higher degree of deformation before fracture. The cantilevered-beam configuration was less suitable for mechanical testing with indentation because of the instabilities of the free end under the AFM probe.

1. Introduction

Nanowires (NWs) are practically important materials for a wide range of emerging applications (Lieber, 2003). NWs possess unique physical properties associated with their highly anisotropic geometry as well as the size effects that suggests using the use of NWs for nanoscale interconnects, sensors, transparent, conductive electrodes in photovoltaic and optoelectronic devices (Xia et al., 2003).

Among other materials, Au NWs attract special attention due to their ease of synthesis, well-defined geometry, and excellent electrical, optical and chemical properties (Takahata et al., 2014; Sanchez-Iglesias et al., 2012; Hong et al., 2014). Au NWs cover many fields of application, such as biosensors (Chen et al., 2013a), gas sensors (Moon et al., 2014), catalysts (Zhu et al., 2014), mechanical energy storage and release (Xu and Jiang, 2014), flexible electrodes (Chen et al., 2013b) and surface-enhanced Raman scattering (Hong et al., 2011; Feng et al., 2009).

In certain applications, e.g. flexible coatings (Lee et al., 2012a; Lee et al., 2012b; Maurer et al., 2016), nanorelays, nanoswitches (Loh and Espinosa, 2012), and nanoresonators (Li et al., 2008), NWs undergo multiple bending deformations. Moreover, in nanophotonics, bending can be a part of the design for guiding the light in the desired direction (Singh et al., 2012). Defects such as cracks occurring in bent-metal NWs can strongly affect the light propagation in waveguides (Wang et al., 2011; Park and Qian, 2010). Therefore, better understanding and control over mechanical properties and development of reliable methods for the mechanical characterisation of NWs that would consider the specific conditions of the particular applications are required.

Depending on the synthesis method and parameters, NWs may have different geometries, inner structures and concentrations of defects that may result in different mechanical properties. For instance, by introducing the ultra-dense twinned structure, it is possible to reach nearly ideal strength (Wang et al., 2013a; Deng and Sansoz, 2009). It was also shown theoretically that Au NWs with a five-fold twinned

* Corresponding author.
E-mail address: sergei.vlassov@ut.ee (S. Vlassov).

https://doi.org/10.1016/j.micron.2019.102686
Received 18 February 2019; Received in revised form 26 May 2019; Accepted 26 May 2019
Available online 08 June 2019
0968-4328/

structure, which is the one of the most common forms of chemically synthesis Au NWs (Chen et al., 2004), can have increased stiffness because of inner anisotropy (Mets et al., 2016). Such NWs consist of five monocrystalline NWs with a triangular cross-section that is connected by twin boundaries. Therefore, by tuning the internal structure, it is possible to modify the mechanical properties of Au NWs. Several theoretical studies of the mechanical properties of Au NWs relate the NW structure to its strength (Diao et al., 2004; Park and Zimmerman, 2005; Jiang and Batra, 2009).

There are several experimental works available for Au NWs (Seo et al., 2011; Wang et al., 2013a; Wu et al., 2005a; Dou and Derby, 2008; Vlassov et al., 2017). The three-point bending test is one of the most popular nanomechanical characterisation methods for 1-D nanostructures. In this method, the central part of the NW is suspended over the cavity while both ends rest on a substrate. The NW is then indented in midpoint with an AFM probe, and the force vs. deformation is recorded. This setup allows the Young's modulus and bending strength to be determined in one measurement. Typically, the NW ends are immovable during the measurements because of high adhesion or additional clamping. However, this approach has certain flaws. The distribution of stresses is highly non-uniform with the most localized stress in the vicinity of the clamp and probe regions. The boundary problem of the three-point bending test has been discussed previously in several works (Chen et al., 2007; Zhang and Zhao, 2011) where researchers focused mainly on the problem of NW adhesion to the substrate. Their results show that depending on the NW or/and substrate surface quality or interface properties, the Young's modulus measured may differ significantly. The problem is complicated if the boundary condition is uncertain. The most known solution is the welding of NW ends by platinum or carbon using FIB-assisted deposition (Jenkins et al., 1991). The drawback is Pt or C material deposition in proximity to the welded region, which may increase the NW radius and the alter mechanical test results.

In this study, we introduced an alternative approach to the three-point bending test where both ends of the NW are free. We compared the free-ends configuration to the fixed-ends and cantilevered configurations. As a test object, we selected a five-fold twinned Au NWs with pentagonal cross-section because their mechanical properties were never characterised experimentally. We measured the elastic modulus in all the three configurations and linked the results to the boundary effects of non-uniform mechanical stress by finite element method (FEM) modelling. In addition, plastic deformation and plastic yield were measured and compared to the FEM modelling results.

2. Results and discussion

2.1. Nanomechanical tests

Freshly synthesised Au NWs were drop-casted from a water solution onto the patterned silicon substrate (see Fig. s1 in Supplementary materials). The scanning electron microscope (SEM) observation revealed uniform NWs with pentagonal cross-section. After the drop-casting procedure, some of the Au NWs were suspended from pyramidal holes in one of the three configurations: free-ends when the NW is positioned diagonally inside the i-pyramid so the ends of the NWs contact the substrate only at a few point (Fig. 1a), fixed-ends when the NW is partly suspended over the rectangular hole with both sides of the NWs resting on the substrate (Fig. 1b), and cantilevered when the NW is half-suspended over the hole (Fig. 1c). The three-point bending method was applied for both the fixed-end and free-end configurations of the Au NWs, and the cantilevered-beam bending technique was applied for the half-suspended NWs (Fig. 1d).

The bending test was performed with atomic force microscope (AFM) by pushing the NW with AFM tip downwards, as shown schematically in Fig. 1d–f. Several force-displacement curves were obtained for each tested NW, and the linear part of the indentation curve was used for calculating Young's modulus using the theoretical curves governed by Eq. 2,3 and 4.

The Young's modulus was measured for 21 Au NWs with the fixed-ends configuration (the most frequently appeared configuration), for 14 NWs in the free-ends configuration and only for 3 NWs in the cantilevered configuration. Low statistics for cantilevered configuration are conditioned by problems associated with measurements. It is difficult to achieve steady conditions and obtain linear force-displacement curves because of the pentagonal cross-section (the tip should indent the NW at the narrow edge) and higher (in comparison to other configurations) degrees of motional freedom that can cause tip slippage along the NW during measurements. Therefore, the cantilevered configuration is less preferable for pentagonal NWs. Alternatively, the probe should move in-plane with the substrate (lateral mode measurements), but our setup does not allow for measurements in lateral mode.

The median elastic moduli measured for the fixed-ends, free-ends and cantilevered configurations were 88 ± 20 GPa, 87 ± 16 GPa and 63 ± 16 GPa, respectively. The obtained Young's modulus values are summarized in Fig. 2. A tendency of increasing the modulus with decreased diameter can be observed. Such dependence is well-known for nanostructures, and the case of elastic properties is related to the increased stiffer surface to the overall elasticity of NWs for smaller diameters (Chen et al., 2006). The size effect also partly explains seemingly high scattering around median values. Either way, the scattering is within an acceptable range, and it is the typical behaviour for nanoscale materials (Wu et al., 2005b). Despite the scattering, the results show that the values for both the free- and fixed-ends configurations fall into the same range. The three-point bending test with fixed ends is well-established and the widely accepted method and the free-ends configuration yielding comparable results indicates that this testing method can be considered as a reliable alternative that has certain advantages. Namely, in the free-end configuration, more uniform deformation and pure bending conditions are realized in contrast to the fixed-ends configuration where stresses are localized in the vicinity of clamping and probe regions. Moreover, the free-ends configuration benefits from more favourable NW position relative to the probe with facet facing upwards in contrast to the sharp edge in the case of fixed ends (see Fig. s2 in Supplementary Materials).

The results show that the measured Young's moduli were noticeably higher than that of the bulk value of Au (78 GPa (Kelly, 2015)). In addition to the surface effect, which is commonly more pronounced below 100 nm, the size dependence could be explained by the anisotropic inner structure of the pentagonal NWs that have internal stresses stored. Mets et al. (2016) also showed that the peculiar structure of pentagonal NWs could lead to higher overall NW stiffness, as the internal structure of the NWs is not considered. The lower elastic modulus values for the cantilevered bending configuration could be explained by the slippage of the AFM tip along the NW during the bending experiments, and this slippage cannot be directly considered because it may vary for different experiments.

In addition to the Young's modulus measurements, the strength measurements were performed on 15 Au NWs in the fixed-ends configuration (Fig. 3). Most technical details for strength measurements are the same as for Young's modulus measurement. The fixed-ends configuration allowed us to increase the displacement of NW and overcome the plastic limit and induce the plastic deformation and fracture of Au NW. The median strength was 1.45 GPa.

Note, that the strength of bulk Au is only up to 210 MPa (Howatson et al., 1972). The high-strength values for NWs indicate that the NWs were of high quality with a relatively low concentration of defects, as was indicated in the works conducted by Wang et al. (2013b).

The uniformity of mechanical properties of pentagonal Au NWs was analysed with Weibull statistics (Barber et al., 2005a; Landau and Lifshitz, 1970). The method is widely used to determine the material's strength distribution that is usually governed by the statistical distribution of critical defects. The Weibull statistic gives the cumulative

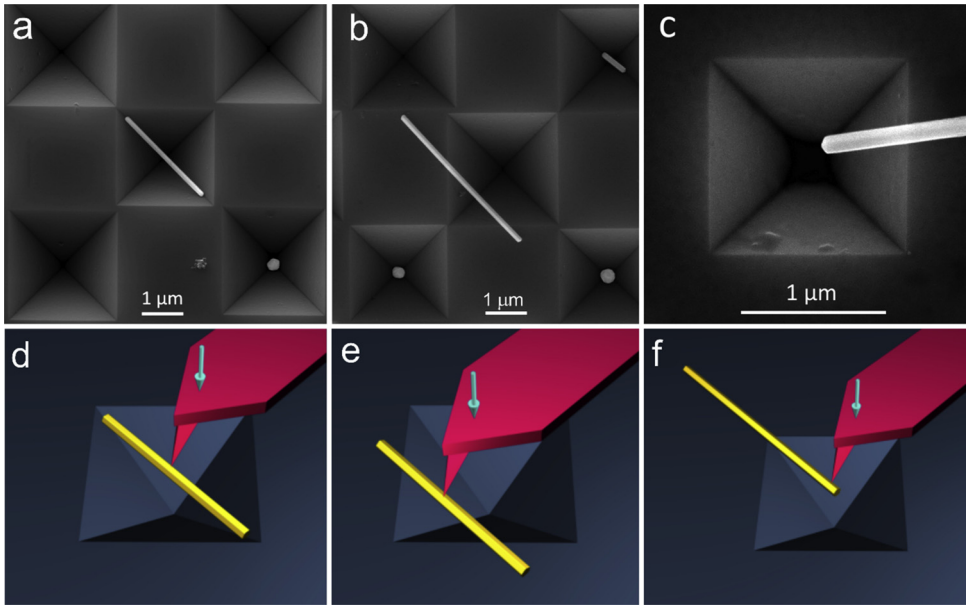

Fig. 1. SEM images and corresponding schematics of Au NWs in three different configurations: free-ends (a,d), fixed-ends (b,e) and cantilevered (c,f).

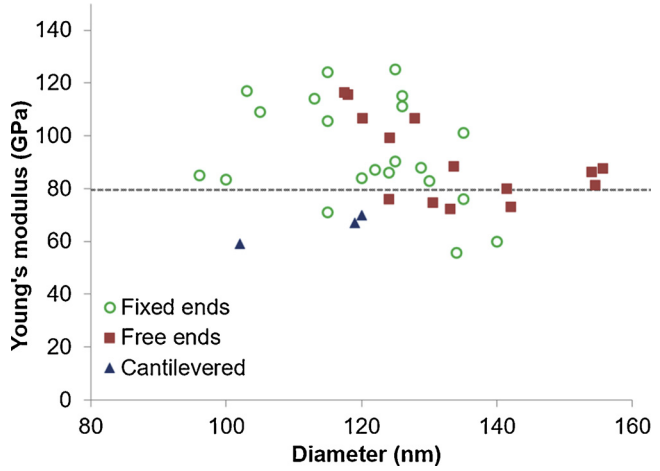

Fig. 2. Young's modulus measured in three configurations: green circles – fixed-ends, red squares – free-ends, blue triangles - cantilevered. (For interpretation of the references to colour in this figure legend, the reader is referred to the web version of this article).

probability distribution of strength P_S at the maximum stress σ_{Ymax} for a sample as follows:

$$P_S = 1 - \exp[-\left(\frac{\sigma_{Ymax}}{\sigma_0}\right)^m] \quad (1)$$

where σ_0 is the strength at which 63% of the samples plastically deform, m is the Weibull modulus, which is a dimensionless parameter used to describe the variation in the measured strength values. A higher m value corresponds to a steeper slope in the Weibull plot and indicates a lower deviation in the strength values.

The Weibull moduli for the strength of Au NWs were 3.3 and 3.7 for FEM and elastic beam theory (EBT) calculations, respectively. High scattering is typical for the nanoscale materials. In comparison, the Weibull modulus reported by (Barber et al. (2005b)) for chemical vapour deposition and arc discharge synthesised multiwall carbon nanotubes were m = 1.7 and m = 2.4, respectively. The Weibull modulus of ZnO and CuO NWs reported by Polyakov et al. (Polyakov et al., 2012) were m ≈ 2 and m ≈ 3, respectively.

2.2. Effect of boundary conditions: FEM modelling

To gain further insight into the effect the boundary conditions on the mechanical response of suspended NWs, all three configurations were simulated and analysed with FEM modelling. Geometrical and elastic parameters were based on averaged experimental data. The diameter was the same for all three configurations, while the length of

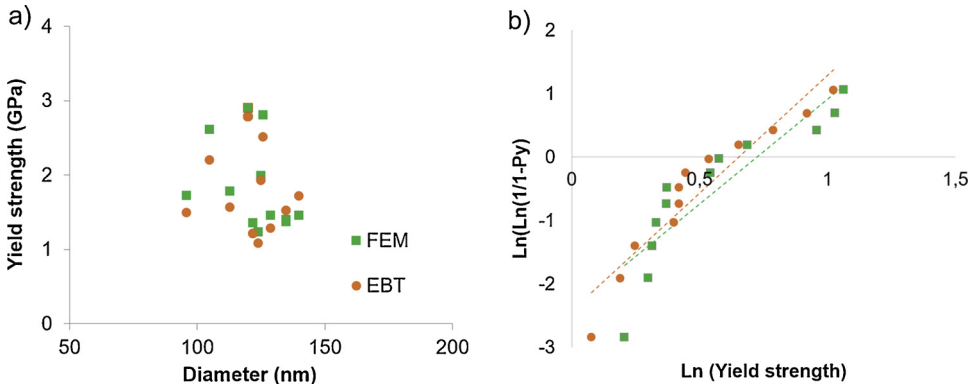

Fig. 3. a) The strength of Au NWs in the fixed-ends configuration. Orange dots correspond to values calculated with EBT. Green squares correspond to FEM calculations. b) Corresponding Weibull statistics. (For interpretation of the references to colour in this figure legend, the reader is referred to the web version of this article).

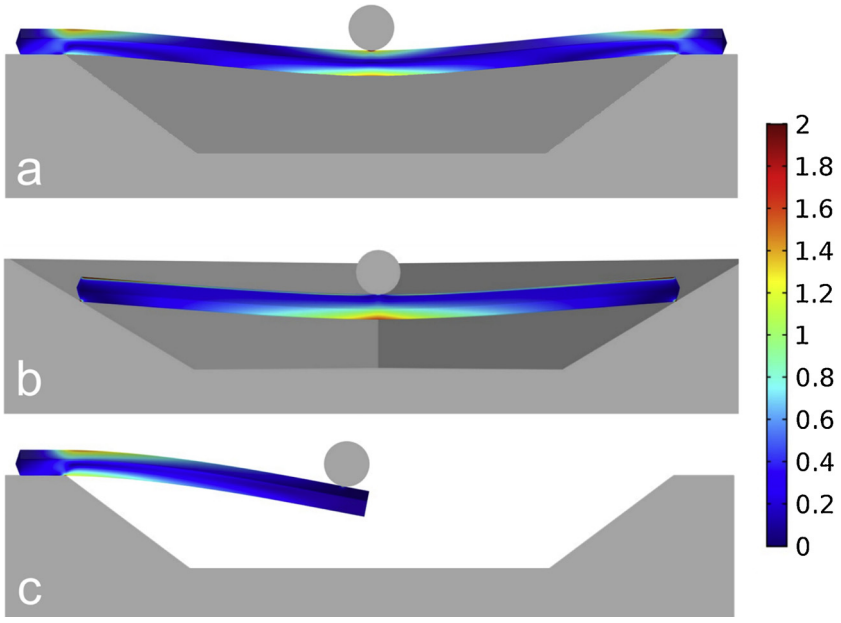

Fig. 4. FEM simulations of An NW bending in three different configurations: three-point bending with fixed ends (a), three-point bending with free ends (b) and cantilever beam bending (c). The colour legend corresponds to Von Mises stress in GPa.

the suspended part was half that chosen for the three-point fixed-ends and free-ends configurations. This was done to keep the point of maximal deformation the same distance from the ends of the NWs and keep the simulation results comparable. The Young's modulus of 88 GPa was used as the median based on experimental data.

The results of the simulations at deflections close to the strength limit of Au NW are shown in Fig. 4, where the distribution of internal stresses (Von Mises stress) is visualized for each configuration.

A key noticeable difference is the large stress exhibited at the fixed boundaries of the cantilevered and fixed three-point configurations. This high stress at the interface might also be high enough to induce plastic failure of the NW during bending. For the cantilevered bending experiment, it is evident, but for the fixed three-point configuration the stress at the middle point was expected to be higher than at the fixed interface. This fact is also supported by the experimental findings, as the NW always broke from the centre. As this result cannot be seen in the simulations, the stress at the centre was lower than at the edges, indicating that in the experiments, the sharp edges of the i-pyramids might have considerable curvature, resulting in the dissipation of stresses in those regions. The high stress at the edges of the NWs can be avoided in the free three-point bending experimental configuration, as the ends are not fixed and exhibit lower tensile stress.

In addition, FEM simulations were used to calculate the strength of NWs in the fixed-ends configuration to compare with results obtained by EBT equations. The results of FEM-based strength measurements are presented in Fig. 3a. The FEM-calculated median strength was 1.52 GPa that is very close to 1.45 GPa calculated with the EBT equation. Such good agreement between the two methods indicates that both approaches are trustworthy. EBT-based calculations are simpler, while FEM is more accurate and benefits form the visualization of stresses.

3. Conclusions

In this work, we measured the mechanical properties of pentagonal gold nanowires in three-point and cantilevered bending tests performed with AFM. The three-point bending test was performed in two configurations: in addition to the standard situation when the nanowire ends are fixed during measurements, we introduced an alternative approach that allowed us to perform measurements with free ends. The median elastic moduli measured for the fixed-ends, free-ends and cantilevered configurations were 88 ± 20 GPa, 87 ± 16 GPa and 63 ± 16 GPa, respectively. The lower values obtained in the cantilevered-beam bending test in comparison to three-point bending are probably related to difficulties in achieving steady conditions and obtaining linear force-displacement curves because of the pentagonal cross-section (the tip should indent the NW at narrow edge) and higher (in comparison to other configurations) degrees of motional freedom that contribute to tip slippage along the NW during measurements. Therefore, the cantilevered configuration is less preferable for pentagonal NWs. Alternatively, the probe should move in-plane with the substrate (lateral mode measurements). However, our setup does not allow for measurements in lateral mode.

Both three-point bending test configurations yield similar results; therefore, the free-end configuration can be considered a reliable alternative to the fixed-end configuration that have certain advantages. Namely, in the free-end configuration, more uniform deformation and pure bending conditions are realized, in contrast to the fixed-ends configuration where stresses are localized in the vicinity of clamping and probe regions. In contrast, the fixed-ends configuration is more suitable for strength measurements as it allowed to achieve rupture of nanowires in the bending test. The median strength value calculated for fixed-ends configuration was 1.45 GPa.

In addition to experimental measurements, all three configurations were simulated with FEM to obtain deeper insight into stress distribution inside NW depending on the test conditions. FEM simulations were also used to calculate the strength of NWs in the fixed-ends configuration and compare them with the results obtained by EBT equations. The FEM-calculated median strength was 1.52 GPa, and that is very close to the EBT-obtained value. Such good agreement between the two methods indicates that both approaches are trustworthy. The EBT-based calculations are simpler, while FEM is more accurate and benefits form visualization of stresses.

Overall, our work contributes to better understanding the mechanical properties of pentagonal gold nanostructures and can help determine proper test conditions for the mechanical characterisation of nanowires.

Acknowledgements

This work was supported by the Estonian Research Council projects

PUT1689 and PUT1372 and the Latvian Science Council grant lzp-2018/2-0083.

Appendix A

Experimental Details

Materials

Gold nanowires were produced from gold seeds in a three-step synthesis process adopted from (Murphy et al., 2005). All chemicals were purchased from Sigma-Aldrich. The growth solution was prepared by mixing 240 ml of 0.2 M hexadecyltrimethylammonium bromide (CTAB) and 10 ml of 0.0001 M of $HAuCl_4$. Afterwards, 1.5 ml of 0.1 M ascorbic acid was added. The growth solution was divided into two 25 ml glass bottles labelled "A" and "B", and 200 ml was placed in vessel "C". Into vessel "C", 0.25 ml of concentrated HNO_3 was added. A volume of 0.2 ml of the citrate stabilized gold seed nanoparticles (approx. 5 nm in diameter) solution was added into bottle "A". Then, 0.2 ml of solution from bottle "A" was transferred to bottle "B". Lastly, 0.1 ml of solution in bottle "B" was then transferred to vessel "C". The solution was kept in at 25 °C temperature for 12 h. The precipitates of gold nanowires were observed on the bottom of the tube after the reaction. The supernatant was poured out of the solution, and the gold nanowires precipitate was redispersed in 5 ml of deionized water. According to the literature and our previous experience, pentagonal nanowires grow along [110] directions with {100} planes terminating all side facets (e.g. Fig. 1 in (Mets et al., 2016)).

Micropatterned silicon substrates with regular rows of pyramidal holes were prepared using standard the silicon micromachining approach. SU-8 negative photoresist was spin-coated onto an oxidized silicon wafer (50 nm SiO_2) from Semiconductor Wafer Inc. (p-type < 100 > , 0.001 O-cm) and exposed by Heidelberg μPG 101 direct-write micropattern generator. After photoresist developing and the hard-baking procedure, the unprotected silicon oxide layer was etched in ammonium fluoride buffered HF. Then, the exposed silicon etched in 25% tetramethylammonium hydroxide solution (TMAH) at 95 °C. Finally, the residual photoresist was removed in hot resist remover. The micropatterned substrates were immersed in concentrated HF to etch away remaining silicon oxide and were rinsed in deionized water. As a result, the substrate had a great number of cavities in the shape of inverted pyramids of different sizes. Such structures are convenient for performing mechanical tests on suspended NWs (Vlassov et al., 2016).

Characterisation and measurements

Prior to the mechanical characterisation, the samples were visualized in a high-resolution SEM (HR-SEM, Helios Nanolab 600, *FEI*) to find proper NWs in appropriate configurations.

The mechanical characterisation of NWs was performed with an AFM (Dimension Edge, *Bruker*) under ambient conditions using silicon AFM Tips (PPP-NCH, *NANOSENSORS*).

After the mechanical testing experiments, the AFM cantilever was characterised in the HR-SEM for obtaining all the geometrical parameters (tip radius, length, width, thickness) necessary for calculating the normal stiffness.

(2) Elastic beam theory

Numerical values of mechanical properties of investigated NWs were obtained with the EBT that is typically used for analysing elastic isotropic beams deformed by an external force. For the three-point bending test configuration with free ends, the force-displacement relationship is governed by the following expression (Zhou et al., 2008):

$$F = \frac{48EI}{L^3}\delta, \tag{2}$$

where δ is the displacement of the centre point, L is the length, E is the Young's modulus, and I is the area moment of inertia of the beam.

The force-displacement relationship for the three-point bending test with fixed ends, where both the elastic bending and tensile strain are considered, is given by the following expression (Gere and Goodo, 2012):

$$F = \frac{192EI}{L^3}\delta\left(1 + \frac{A}{24I}\delta^2\right), \tag{3}$$

where A is the area of the cross-section of the beam.

For the cantilevered-beam bending configuration, the force-displacement is given by the following relationship (Heidelberg et al., 2006):

$$F = \frac{3EI}{L^3}\delta. \tag{4}$$

For a pentagonal beam, the area moment of inertia can be expressed as:

$$I = \frac{1}{96}\frac{(3-\sqrt{5})}{(3+\sqrt{5})}\sqrt{265+118\sqrt{5}}\,D^4, \tag{5}$$

where D is the apparent diameter of the beam measured from the SEM micrographs.

In the linear elastic regime and small displacements, depending on configuration, the Young's modulus can be expressed as:

$E = k_{TPB}\frac{L^3}{48I}$ and $E = k_{TPB}\frac{L^3}{192I}$, $E = k_{TPB}\frac{L^3}{3I}$ for free-ends, fixed-ends and the cantilevered configurations, respectively, where $k_{TPB}$is the stiffness of the beam measured from the AFM bending experiments.

(6) Finite element method

In addition to the experimental AFM bending measurements, the same conditions were simulated using the FEM (COMSOL Multiphysics 5.2) for visualizing the stress distribution of the different systems. The simulations combined the elastic deformation of NWs with the contact modelling of the substrate, NW and indenter. Because very large deformations of the NWs were observed, finite strain theory was utilised. As such, the material

deformation follows Green-Lagrange strain (ε), calculated as:

$$\varepsilon = \frac{1}{2}(F^T F - I), \tag{6}$$

where F is the deformation gradient tensor linking the deformed and non-deformed configurations by $x_i = F_{ij}X_j$. Because of the finite strain theory, the material response is presented by second Piola-Kirchoff stress (S), calculated as

$$S = C\colon \varepsilon_{el}. \tag{7}$$

Cauchy stress (σ), the first Piola-Kirchoff stress (P) and the second Piola-Kirchoff stress are related by $S = F^{-1}P$ and $\sigma = J^{-1}PF^T = J^{-1}FSF^T$, with $J = \det(F) = V/V_0$ being the ratio between the deformed and non-deformed volumes (Bower, 2009)

The contact modelling was distributed into two cases. The first scenario covered NW-indenter and the second NW-substrate contact. The NW-indenter interaction was always solved using penalty factor contact pair approach, which is readily available in Comsol Multiphysics. NW-substrate pair was solved using either the zero displacements boundary condition (fixed NW, Fig. 4 a, c) or as a second penalty factor contact pair (Fig. 4 b).

The solution procedure utilised parametric solver, in conjunction with damped Newton-type method (Deuflhard, 1974) and MUMPS (http://graal.ens-lyon.fr/MUMPS/) linear solver, was configured for the gradual lowering of the indenter for continuous deformation of the simulated NW. In all simulations, the indenter was lowered for 200 nm so that the maximum observed stress in the wire reached 2 GPa as a stopping condition. The finite element mesh used to represent the NW consisted of ˜32 000 hexagonal elements with linear shape functions that were obtained using the swept mesh technique with finer mesh near the contact areas.

Appendix B. Supplementary data

Supplementary material related to this article can be found, in the online version, at doi:https://doi.org/10.1016/j.micron.2019.102686.

References

C.M. Lieber, MRS Bulletin 2003. 28, 486. https://doi.org/10.1557/mrs2003.144.

Xia, Y.N., Yang, P.D., Sun, Y., Wu, Y.Y., Mayers, B., Gates, B., Yin, Y.D., Kim, F., Yan, H.Q., 2003. Adv. Mater. 15, 353. https://doi.org/10.1002/adma.200390087.

Takahata, R., Yamazoe, S., Koyasu, K., Tsukuda, T., 2014. J. Am. Chem. Soc. 136, 8489. https://doi.org/10.1021/ja503558c.

Sanchez-Iglesias, A., Rivas-Murias, B., Grzelczak, M., Perez-Juste, J., Liz-Marzan, L.M., Rivadulla, F., Correa-Duarte, M.A., 2012. Nano Lett. 12, 6066. https://doi.org/10.1021/nl3021522.

Hong, X., Tan, C.L., Chen, J.Z., Xu, Z.C., Zhang, H., 2014. Nano Res. 8, 40. https://doi.org/10.1007/s12274-014-0636-3.

Chen, Y.L., Lee, C.Y., Chiu, H.T., 2013a. J. Mater. Chem. B 1, 186. https://doi.org/10.1039/C5TB00266D.

Moon, C.H., Zhang, M., Myung, N.V., Haberer, E.D., 2014. Nanotechnology 25, 1. https://doi.org/10.1088/0957-4484/25/13/135205.

Zhu, W.L., Zhang, Y.J., Zhang, H.Y., Lv, H.F., Li, Q., Michalsky, R., Peterson, A.A., Sun, S.H., 2014. J. Am. Chem. Soc. 136, 16132. https://doi.org/10.1021/ja5095099.

Xu, J.P., Jiang, W., 2014. Macromolecules 47, 2396. https://doi.org/10.1021/ma5003485.

Chen, Y., Ouyang, Z., Gu, M., Cheng, W.L., 2013b. Adv. Mater. 25, 80. https://doi.org/10.1002/adma.201202241.

Hong, X., Wang, D.S., Li, Y.D., 2011. Chem. Commun. 47, 9909. https://doi.org/10.1039/C1CC13651H.

Feng, H.J., Yang, Y.M., You, Y.M., Li, G.P., Guo, J., Yu, T., Shen, Z.X., Wu, T., Xing, B.G., 2009. Chem. Commun. 1984. https://doi.org/10.1039/C1CC10903K.

Lee, P., Lee, J., Lee, H., Yeo, J., Hong, S., Nam, K.H., Lee, D., Lee, S.S., Ko, S.H., 2012a. Adv. Mater. 24 (25), 3326–3332. https://doi.org/10.1002/adma.201200359.

Lee, J., Lee, P., Lee, H., Lee, D., Lee, S.S., Ko, S.H., 2012b. Nanoscale 4, 6408–6414. https://doi.org/10.1039/c2nr31254a.

Maurer, J.H.M., González-García, L., Reiser, B., Kanelidis, I., Kraus, T., 2016. Nanoletters. https://doi.org/10.1021/acs.nanolett.5b04319.

Loh, O.Y., Espinosa, H.D., 2012. Nat. Nanotechnol. 7 (5), 283–295. https://doi.org/10.1038/nnano.2012.40.

Li, M., Bhiladvala, R.B., Morrow, T.J., Sioss, J.A., Lew, K.–K., Redwing, J.M., Keating, C.D., Mayer, T.S., 2008. Nat. Nanotechnol. 3 (2), 88–92. https://doi.org/10.1038/nnano.2008.26.

Singh, D., Raghuwanshi, M., Pavan Kumar, G.V., 2012. Appl. Phys. Lett. 101, 111111. https://doi.org/10.1063/1.4824896.

Wang, W., Yang, Q., Fan, F., Xu, H., Wang, Z.L., 2011. Nano Lett. 11 (4), 1603–1608. https://doi.org/10.1038/srep08469.

Park, H.S., Qian, X.J., 2010. Phys. Chem. C 114 (19), 8741–8748. https://doi.org/10.1021/jp104317x.

Wang, J., Sansoz, F., Huang, J., Liu, Y., Sun, S., Zhang, Z., Mao, S.X., 2013a. Nat. Commun. 4, 1742. https://doi.org/10.1038/ncomms2768.

Deng, C., Sansoz, F., 2009. ACS Nano 3 (10). https://doi.org/10.1021/nn900668p.

Chen, H., Gao, Y., Zhang, H., Liu, L., Yu, H., Tian, H., Xie, S., Li, J., 2004. J. Phys. Chem. B 108, 12038–12043. https://doi.org/10.1021/jp048023d.

Mets, M., Antsov, M., Zadin, V., Dorogin, L.M., Aabloo, A., Polyakov, B., Lõhmus, R., Vlassov, S., 2016. Phys. Scr. 91, 115701. https://doi.org/10.1088/0031-8949/91/11/115701. (7pp).

Diao, J.K., Gall, K., Dunn, M.L., 2004. J. Mech. Phys. Solids 52, 1935. https://doi.org/10.1016/j.jmps.2004.03.009.

Park, H.S., Zimmerman, J.A., 2005. Phys. Rev. B 72, 054106. https://doi.org/10.1103/PhysRevB.72.054106.

Jiang, W., Batra, R.C., 2009. Acta Mater. 57, 4921. https://doi.org/10.1016/j.actamat.2009.06.062.

Seo, J.H., Yoo, Y., Park, N.Y., Yoon, S.W., Lee, H., Han, S., Lee, S.W., Seong, T.Y., Lee, S.C., Lee, K.B., Cha, P.R., Park, H.S., Kim, B., Ahn, J.P., 2011. Nano Lett. 11 (8), 3499–3502. https://doi.org/10.1021/nl2022306.

Wu, B., Heidelberg, A., Boland, J.J., 2005a. Nat. Mater. 4, 525–529. https://doi.org/10.1038/nmat1403.

Dou, R., Derby, B., 2008. Scr. Mater. 59, 151–154. https://doi.org/10.1016/j.scriptamat.2008.02.046.

Vlassov, S., Polyakov, B., Vahtrus, M., Mets, M., Antsov, M., Oras, S., Tarre, A., Arroval, T., Lõhmus, R., Aarik, J., 2017. Nanotechnology 28 (50), 505707. https://doi.org/10.1088/1361-6528/aa973c.

Chen, Y., Stevenson, I., Pouy, R., Wang, L., Mcllroy, D.N., Pounds, T., Norton, M.G., Aston, D.E., 2007. Nanotechnology 18, 135708. https://doi.org/10.1088/0957-4484/18/13/135708.

Zhang, Y., Zhao, Y.P., 2011. J. Adhes. Sci. Technol. 25 (10), 1107–1129. https://doi.org/10.1163/016942410X549898.

Jenkins, D.W.K., Allen, G.C., Prewett, P.D., Heard, P.J., 1991. Phys. :Condens. Matter 3, S199–S206. https://doi.org/10.1088/0953-8984/3/S/032.

Chen, C.Q., Shi, Y., Zhang, Y.S., Zhu, J., Yan, Y.J., 2006. Phys. Rev. Lett. 96, 075505. https://doi.org/10.1103/PhysRevLett.96.075505.

Wu, B., Heidelberg, A., Boland, J.J., 2005b. Nat. Mater. 4 (July). https://doi.org/10.1038/nmat1403. DOI: 10.1038/nmat1403.

Kelly, P.F., 2015. Properties of Materials. CRC Press, pp. 355 ISBN 978-1-4822-0624-1.

Howatson, A.M., Lund, P.G., Todd, J.D., 1972. Engineering Tables and Data. p. 43, ISBN 0412115506. .

Wang, J., et al., 2013b. Near-ideal theoretical strength in gold nanowires containing angstrom scale twins. Nat. Commun. 4, 1742. https://doi.org/10.1038/ncomms2768.

Barber, A.H., Kaplan-Ashiri, I., Cohen, S.R., Tenne, R., Wagner, H.D., 2005a. Sci. Technol. 65, 2380–2384. https://doi.org/10.1016/j.compscitech.2005.07.021.

Landau, L.D., Lifshitz, E.M., 1970. Theory of Elasticity. Pergamon Press, Oxford ISBN 0080064655.

Barber, A.H., Andrews, R., Schadler, L.S., Wagner, H.D., 2005b. Appl. Phys. Lett. 87, 203106. https://doi.org/10.1063/1.2130713.

Polyakov, B., Dorogin, L., Vlassov, S., et al., 2012. Eur. Phys. J. B 85, 366. https://doi.org/10.1140/epjb/e2012-30430-6.

Murphy, C.J., Sau, T.K., Gole, A.M., Orendorff, C.J., Gao, J., Gou, L., Hunyadi, S.E., Li, T., 2005. J. Phys. Chem. B 109, 13857–13870. https://doi.org/10.1021/jp0516846.

Vlassov, S., Polyakov, B., Oras, S., Vahtrus, M., Antsov, M., Šutka, A., Smits, K., Dorogin, L.M., Lõhmus, R., 2016. Nanotechnology 27 (33). https://doi.org/10.1088/0957-4484/27/33/335701.

Zhou, P., Wu, C., Li, X., 2008. Meas. Sci. Technol. 19, 115703. https://doi.org/10.1088/0957-0233/19/11/115703. 5p.

Gere, J., Goodo, B., 2012. Mechanics of Materials, Brief Edition, SI Version. Cengage Learning, Stamford, CT, USA ISBN-13: 978-1-111-13602-4.

Heidelberg, A., Ngo, L.T., Wu, B., Phillips, M.A., Sharma, S., Kamins, T.I., Sader, J.E., Boland, J.J., 2006. Nano Lett. 6, 1101–1106. https://doi.org/10.1021/nl060028u.

Bower, A.F., 2009. Applied mechanics of solids, CRC press. In: Ottosen, N.S., Ristinmaa, M. (Eds.), The Mechanics of Constitutive Modeling. Elsevier, pp. 2005.

Deuflhard, P., 1974. Numer. Math. 22, 289–315. https://doi.org/10.1007/BF01406969.